Published December 27, 1999

Cingulin Contains Globular and Coiled-coil Domains and Interacts with ZO-1, ZO-2, ZO-3, and Myosin

Michelangelo Cordenonsi,* Fabio D'Atri,‡§ Eva Hammar,§ David A.D. Parry,‖ John Kendrick-Jones,¶ David Shore,§ and Sandra Citi*§

*Department of Biology, University of Padova, 35121 Padova, Italy; ‡Department of Biochemistry and §Department of Molecular Biology, University of Geneva, 1211 Geneva 4, Switzerland; ‖Institute of Fundamental Sciences, Massey University, Palmerston North, New Zealand; and ¶Medical Research Council Laboratory of Molecular Biology, Cambridge, CB22QH UK

Abstract. We characterized the sequence and protein interactions of cingulin, an M_r 140–160-kD phosphoprotein localized on the cytoplasmic surface of epithelial tight junctions (TJ). The derived amino acid sequence of a full-length *Xenopus laevis* cingulin cDNA shows globular head (residues 1–439) and tail (1,326–1,368) domains and a central α-helical rod domain (440–1,325). Sequence analysis, electron microscopy, and pull-down assays indicate that the cingulin rod is responsible for the formation of coiled-coil parallel dimers, which can further aggregate through intermolecular interactions. Pull-down assays from epithelial, insect cell, and reticulocyte lysates show that an NH_2-terminal fragment of cingulin (1–378) interacts in vitro with ZO-1 (K_d ~5 nM), ZO-2, ZO-3, myosin, and AF-6, but not with symplekin, and a COOH-terminal fragment (377–1,368) interacts with myosin and ZO-3. ZO-1 and ZO-2 immunoprecipitates contain cingulin, suggesting in vivo interactions. Full-length cingulin, but not NH_2-terminal and COOH-terminal fragments, colocalizes with endogenous cingulin in transfected MDCK cells, indicating that sequences within both head and rod domains are required for TJ localization. We propose that cingulin is a functionally important component of TJ, linking the submembrane plaque domain of TJ to the actomyosin cytoskeleton.

Key words: cingulin • tight junction • epithelia • MDCK • protein

EPITHELIAL and endothelial cell sheets form semipermeable barriers to the passage of cells, molecules, and ions across two compartments of the extracellular space. To achieve this barrier function, cells develop a circumferential seal around the apical pole of the cell, which is part of the junctional complex (Farquhar and Palade, 1963) and is called tight junction (TJ)[1] or zonula occludens. TJ can finely regulate the passage of molecules through the paracellular pathway (gate function) and are also located precisely at the boundary between distinct apical and basolateral domains of the plasma membranes of polarized epithelial and endothelial cells (fence function). Thus, TJ have a key role in the function of all epithelia involved in polarized secretion or absorption and in the formation of barriers between different tissue and organ compartments. Furthermore, TJ can be targets of toxins, and TJ modulation may be important in the pathogenesis of disease and in the therapeutic delivery of drugs across physiological barriers (De Boer and Breimer, 1994; Schneeberger, 1994). As a result, TJ have been extensively studied at the morphological, functional, and molecular levels.

Several studies have contributed to elucidate the molecular structure of TJ (for review see Citi and Cordenonsi, 1998; Mitic and Anderson, 1998; Stevenson and Keon, 1998). The plasma membrane of TJ contains at least three distinct sets of integral membrane proteins, occludin (M_r 58–82 kD) (Furuse et al., 1993), claudins (M_r 22 kD) (Furuse et al., 1998), and JAM (M_r 36–41 kD) (Martin-Padura et al., 1998). Mouse embryonic stem cells lacking occludin show normal TJ, indicating that occludin is not essential for TJ organization and function (Saitou et al., 1998). In the cytoplasm immediately beneath the TJ membrane, there are a number of proteins, most of which have been immunolocalized at the level of TJ by electron microscopy. Such TJ cytoplasmic plaque proteins include ZO-1 (M_r 220 kD) (Stevenson et al., 1986; Itoh et al., 1991, 1993; Willott et al., 1993), ZO-2 (M_r 160 kD) (Gumbiner et al., 1991; Jesaitis and Goodenough, 1994; Beatch et al., 1996),

Address correspondence to Sandra Citi, Department of Molecular Biology, University of Geneva, 30 Quai Ernest Ansermet, 1211 Geneva 4, Switzerland. Tel.: 41-22-7026182. Fax: 41-22-7026868. E-mail sandra.citi@molbio.unige.ch

1. *Abbreviations used in this paper:* GST, glutathione-S-transferase; TJ, tight junction(s).

Published December 27, 1999

and p130/ZO-3 (M_r 130 kD) (Balda et al., 1993; Haskins et al., 1998). These three proteins belong to the membrane-associated guanylate kinase family of proteins since they contain three PDZ domains, followed by one SH3 and one GuK domain, in their NH_2-terminal region. However, they differ in the length and sequence of their COOH-terminal regions, suggesting that they are not functionally redundant. Symplekin (M_r 150 kD) is localized in the cytoplasmic plaque of TJ and in the nucleus of polarized cells and of cells devoid of junctions (Keon et al., 1996). AF-6/afadin (Prasad et al., 1993) is localized at adherens-type junctions (Mandai et al., 1997) and TJ (Yamamoto et al., 1997), and contains one PDZ domain, which is believed to target it to sites of cell–cell contact, and one Ras-binding domain, which mediates interaction with ZO-1 (Yamamoto et al., 1997). Mouse embryos lacking AF-6 lose neuroepithelial polarity and die at embryonic day 10, although ZO-1–containing junctions were detected in mutants (Zhadanov et al., 1999). Despite the fact that the molecular organization of TJ is now much clearer, little direct information is available on the roles that these proteins play in the barrier, gate, and fence functions of TJ.

Cingulin is a protein component of the cytoplasmic plaque of TJ, and was identified by mAbs that recognized a protein copurifying with myosin from chicken intestinal epithelial cells (Citi et al., 1988, 1989). Cingulin is distributed in all polarized epithelia studied so far, and some endothelia, and was localized to the cytoplasmic face of TJ by immunoelectron microscopy (Citi et al., 1988, 1989). In early vertebrate development, cingulin is maternally supplied, and becomes localized at junctional sites at the 8–16-cell stage in mouse preimplantation embryos (Fleming et al., 1993), and at the 2-cell stage in *Xenopus* embryos (Cardellini et al., 1996). Cingulin displays an apparent molecular size of M_r 140 kD in several vertebrate epithelia (for review see Citi, 1994), and M_r 160 kD in *Xenopus laevis* (Cardellini et al., 1996). An M_r 108-kD fragment of chicken cingulin was purified to homogeneity, and was shown to be a highly asymmetric dimer, with a shape, amino acid composition, and biochemical properties consistent with a coiled-coil structure (Citi et al., 1988). Sequencing of a partial cDNA of chicken cingulin confirmed that the amino acid sequence is consistent with a coiled-coil structure (Citi, 1994).

To begin to understand the role of cingulin in TJ, we have isolated and characterized a complete cDNA coding for cingulin from *Xenopus laevis*, and examined the protein interactions of cingulin in vitro and the role of different regions of the molecule in its subcellular localization in vivo. The results show that cingulin interacts in vitro with several of the known protein constituents of TJ and that sequences in both the NH_2-terminal globular region and in the central coiled-coil region are required for TJ localization of cingulin.

Materials and Methods

Antibodies

Rabbit polyclonal anticingulin antiserum C532 was generated against a 45-kD bacterially expressed protein encoding a portion of the COOH-terminal domain of chicken cingulin (Cardellini et al., 1996), and was used at 1:500 for immunofluorescence, and 1:5,000 for immunoblotting and library screening. Rabbit polyclonal anticingulin antiserum R902 was generated in a New Zealand white rabbit by subcutaneous injection of a recombinant fusion protein consisting of GST fused to *Xenopus laevis* cingulin residues 1–378 (GST-XC [1–378)]; see below) and was used at 1:1,000 for immunofluorescence. Other antibodies used for immunoblotting were as follows: rabbit polyclonal antimyosin antiserum R131 (Citi and Kendrick-Jones, 1987; 1:1,000); rabbit polyclonal antibodies against ZO-1 and ZO-2 (Zymed; 1:2,500); mouse mAbs against AF-6 and symplekin (Transduction Laboratories; 1:250); rat mAb R40.76 against ZO-1 (a gift of Dr. D. Goodenough, Harvard University, Boston, MA) (undiluted culture supernatant); and alkaline phosphatase–labeled secondary antibodies (Promega Corp.; 1:7,500). Other antibodies used for immunofluorescence were as follows: undiluted culture supernatant from 9E10 hybridomas; and FITC- or TRITC-labeled secondary antibodies (Jackson Laboratories; 1:100).

cDNA Library Screening and DNA Sequencing

An expression library of *Xenopus laevis* oocyte in λgt11 (cat. no. ZL5000b; CLONTECH Laboratories) was screened with antiserum C532. 10^6 plaques were screened, and three positive phages giving strong immunoreactivity contained the same insert after digestion of DNA with EcoRI. The cDNA insert contained an internal EcoRI site, giving one fragment of ~1.2 kb and one fragment of ~4.0 kb. These two fragments were subcloned into pSK^+ and pKS^+, respectively, and the resulting plasmids (called D902 and D898) were used to prepare constructs either by direct subcloning or PCR amplification. The nucleotide sequence of the cDNA inserts was determined on both strands by cycle sequencing using FS *Taq* polymerase (Perkin-Elmer). The 1,248-bp fragment (D902) contained a 114-bp noncoding region followed by a 1,134-bp open reading frame. The 3,948-bp fragment (D898) contained a 2,976-bp open reading frame followed by a 972-bp noncoding region. It was concluded that in the original cDNA insert, the ~1.2-kb fragment must be located 5′ with respect to the ~4.0-kb fragment. The two fragments joined by the EcoRI site formed a 4,104-bp-long open reading frame.

Protein Sequence Analysis

Cingulin sequence was analyzed with Kyte-Doolitle (DNAStrider1.3) and MacStripe programs (Knight, 1994) (http://www.york.ac.uk/depts/biol/web/homes.htm) to generate plots of predicted hydrophobicity and coiled-coil structure, respectively. PSORT and ScanProsite programs (http://expasy.hcuge.ch) were used to identify sorting signals and other sequence features, and BLAST version 2.0 was used to identify homologies with other proteins.

The heptad-containing region in the amino acid sequence of cingulin was delineated by hand rather than by computer since the former technique is more sensitive to locating discontinuities that may exist in the heptad phasing. Secondary structure analysis was carried out using the Robson (Garnier et al., 1978) and Chou-Fasman techniques (Chou and Fasman, 1978). Potential interchain ionic interactions between charged residue pairs in positions 2e′-1g, 1g′-2e, 2a′-1g, 1g′-2a, 1e′-1d, and 1d′-1e were calculated as a function of relative chain stagger and chain polarity (McLachlan and Stewart, 1975; Parry et al., 1977).

Cell Culture and Preparation of Cell Lysates

Mammalian cells were cultured in a humidified incubator at 37°C and 6% CO_2. MDCK II (a gift of Dr. K. Simons, European Molecular Biology Laboratory, Heidelberg, Germany) and 9E10 hybridoma cells (a gift of Dr. G. Evan, Imperial Cancer Research Fund, London) were grown in DME supplemented with 2 mM glutamine and 10% FBS (Hyclone), CaCo2 cells (a gift of Dr. A. LeBivic, University of Marseille, Marseille, France) in DME supplemented with 2 mM glutamine, 20% FBS, 1% nonessential amino acids, 5 U/ml penicillin/streptomycin; insect cells (Sf21) at 30°C in liquid culture in TC100 supplemented with 10% FBS, and 5 U/ml penicillin/streptomycin.

To prepare lysates for glutathione-S-transferase (GST) pull-down assays, confluent epithelial monolayers or Sf21 cells (30 h after infection at an initial density 0.5×10^6 cells/ml with mouse ZO-1 virus stock, virus provided by Dr. M. Itoh, Kyoto University, Kyoto, Japan) were rinsed twice with cold PBS (140 mM NaCl, 2.7 mM KCl, 10 mM Na_2HPO_4, 1.8 mM KH_2PO_4, pH 7.3), and were lysed in lysis-buffer-triton (LBT: 150 mM NaCl, 20 mM Tris-HCl, pH 7.5, 5 mM EDTA, 1% Triton X-100, 1 mM DTT, 1 mM PMSF, 5 μg/ml leupeptin, 5 μg/ml antipain, 5 μg/ml pep-

Published December 27, 1999

statin) for 30 min with gentle rocking at 4°C. Lysates were clarified by centrifugation at 10,000 *g* at 4°C, and supernatants were used for GST pull-down assays.

To prepare cell lysates for immunoprecipitation, confluent CaCo2 monolayers were rinsed twice with cold PBS, and lysed in CSK buffer (50 mM NaCl, 300 mM sucrose, 10 mM Pipes, pH 6.8, 3 mM $MgCl_2$, 0.5% Triton X-100, 1 mM PMSF, 0.01 mg/ml DNase, 0.01 mg/ml RNase) for 20 min with gentle rocking at 4°C. The supernatants after centrifugation (10 min at 10,000 *g* at 4°C) were the Triton-soluble pool (Caco-T). The pellets were resuspended in one tenth the original volume with SDS immunoprecipitation buffer (1% SDS, 10 mM Tris-HCl, pH 7.5, 2 mM EDTA, 0.5 mM DTT, 0.5 mM PMSF), and solubilized by pipetting and incubating at 100°C for 5 min. To this solubilized sample CSK buffer was added (nine tenths the original lysate volume) to prepare the SDS-soluble pool (CaCo-S).

In Vitro Transcription and Translation

In vitro transcribed and translated proteins were obtained using the TNT T7/T3–coupled reticulocyte system (Promega Corp.), according to the manufacturer's instructions. The full-length human ZO-1 cDNA in pSK^+ (Willott et al., 1993) was a gift of Dr. J. Anderson (Yale University, New Haven, CT). The full-length canine ZO-2 cDNA in pSK^+ (Beatch et al., 1996) was a gift of Dr. D. Goodenough (Harvard University, Boston, MA). A canine ZO-3 cDNA in pSK^+ (Haskins et al., 1998) was a gift of Dr. B. Stevenson (University of Alberta, Edmonton, Canada). The full-length chicken enterocyte myosin II cDNA in pKS^+ (Shohet et al., 1989) was a gift of Dr. R. Adelstein (National Institutes of Health, Bethesda, MD). The full-length *Xenopus* cingulin clone was the construct in pcDNA3.1 (see below). Labeled proteins (5–10 μl) were diluted into LBT (1.5 ml) for GST pull-down assays.

Bacterial Expression of GST Fusion Proteins and GST Pull-down Assays

Constructs for bacterial expression of cingulin fragments were made in pGEX vectors (Pharmacia). GST-XC(1-378) was obtained by subcloning a PCR fragment (amplified from D902 with primers forward 5′-AAGGAATTCATGGAAAGGGATATATATGGCG-3′ and reverse 5′-GAGGAATTCACTCTGGACAGTTCTT-3′) into the EcoRI site of pGEX-1. GST-XC(377-1,368) was obtained by directly subcloning the 3,948-bp EcoRI insert of D898 into the EcoRI site of pGEX4T1. GST-HuZO-1 (849-1,060) was a gift of Dr. J. Anderson and comprises part of the acidic domain, the spliced α-domain, and part of the proline-rich domain of human ZO-1. The production and purification of GST fusion proteins and GST pull-down assays were as described previously (Cordenonsi et al., 1997).

The reticulocyte lysates and uninfected insect cell lysates were tested by immunoblotting with commercial antibodies against ZO-1, ZO-2, ZO-3 (Chemicon International, Inc.), occludin (Zymed Labs), AF-6, and symplekin (see above). No specific cross-reactivity with polypeptides of the expected mobility was seen, except for the presence of an ~200-kD polypeptide in reticulocyte lysates, recognized weakly by the anti–ZO-1 antibodies. However, such reactivity was not detected when the lysate was affinity-purified on GST-XC(1-378) coupled to glutathione-Sepharose.

To measure the dissociation constant between GST-XC(1-378)and ZO-1, Sf21 cells were infected with mouse ZO-1 baculovirus stock, and lysed as described above. GST-XC(1-378) (2.5 μg) was incubated with increasing amounts of Sf21 lysate (containing between 375–9,375 ng total ZO-1 in 1.5 ml), and the amount of ZO-1 bound to agarose beads was quantitated by scanning and analysis (using Biosoft Quantiscan 2.1 software) of Coomassie-stained bands compared with standards of BSA (100–1,000-ng range) in the same gel. The amount of ZO-1 in Sf21 lysates was determined by analysis of Coomassie-stained ZO-1 polypeptide in the lysate (compared with BSA) and by comparing the intensity of the ZO-1 immunoblot in lysates and in pull-downs containing known amounts of ZO-1. Both methods gave similar results (7.5 ng ZO-1 per microliter of lysate). The dissociation constant's K_d value was obtained from a Scatchard plot of the data from two distinct representative experiments.

Immunoprecipitation

Samples of Triton-soluble (CaCo-T) or SDS-soluble (CaCo-S) CaCo2 cell lysates (0.5 ml) were precleared with 100 μl Pansorbin cells (Calbiochem-Novabiochem Corp.) for 1 h at 4°C with gentle rotation. Pansorbin cells were removed by centrifugation at 10,000 *g* for 5 min, and anti–ZO-1 and anti–ZO-2 antibodies (5 μg per sample) or anticingulin C532 antiserum (5 μl per sample) were added to the supernatants. After a 2-h incubation at 4°C, 50 μl of 50% protein A–Sepharose (Pharmacia) beads suspension were added, and incubated for further 4–12 h. Beads were washed 2× with LBT, 2× with wash buffer 1 (WB1: 150 mM NaCl, 20 mM Tris-HCl, pH 7.5, 5 mM EDTA, 0.5% Triton X-100, 0.1% SDS), 2× with wash buffer 2 (WB2: 500 mM NaCl, 20 mM Tris-HCl, pH 7.5, 0.5% Triton X-100), resuspended in SDS sample buffer, and boiled for 3 min before electrophoresis and immunoblotting. 20 μl of cell lysate was run as a positive control for immunoblots.

Transfection

For transfections of cingulin we used pcDNA3.1Myc/His vector (Invitrogen Corp.), which allows the fusion of a Myc-His tag to the COOH-terminal end of the protein. XC(1-1,368)-myc was obtained by ligating two PCR fragments into XbaI-HindIII cut vector. The first fragment was obtained from D902 using as the primers forward 5′-GAGGCTAGCTCTAGACCAACCATGGAAAGGGATATATATGGCG-3′ and reverse 5′-GAGGAATTCACTCTGGACAGTTCTT-3′. The second fragment was obtained from D898 using the primers forward 5′-GAGGAATTCCAGCTGAAAAGTACCC-3′ and reverse 5′-GAGAAGCTTGCATGAGCTGGTCTGCAGG-3′. XC(1-378)–myc was obtained by ligating the PCR fragment obtained from D902 (with primers forward 5′-GAGTCTAGACCAACCATGGAAAGGGATATATATGGCG-3′ and reverse 5′-GAGGAATTCACTCTGGACAGTTCTT-3′) into XbaI-EcoRI cut vector. XC(377-1,368)–myc was obtained by ligating the PCR fragment obtained from D898 (with primers forward 5′-GAGGCTAGCTCTAGACCAACCATGCAGCTGAAAACCCCAGAT-3′ and reverse 5′-GAGAAGCTTGCATGAGCTGGTCTGCAGG-3′) into XbaI-HindIII cut vector. The identity of the clones was checked by restriction digestion and confirmed by DNA sequencing.

For transient transfections, confluent cultures of MDCK cells were trypsinized, and 10^6 cells were plated on glass coverslips in a 10-cm diameter petri dish and transfected 15 h later by the calcium phosphate method (modification of the method described in Graham and van der Eb, 1973) using 40 μg DNA per dish. Cells on coverslips were fixed and stained for immunofluorescence 24–48 h after transfection.

Microinjection of Xenopus laevis Embryos

Constructs for microinjection into *Xenopus laevis* embryos were prepared in the vector pCS2 (Rupp et al., 1994). XC(377-1,368)–myc was obtained by PCR of the construct in pcDNA3.1Myc/His (using primers forward 5′-GAGGAATTCATGCAGCTGAAAAGTACCCCAG-3′, reverse 5′-GAGGAATTCTCAATGATGATGATGATGATGGTC-3′) and subcloning this fragment into EcoRI cut pCS2 vector. XC(1-378) in pCS2 was obtained by ligating the EcoRI insert of D902 with EcoRI cut pCS2 vector.

Xenopus laevis embryos were obtained and dejellied as described previously (Cordenonsi et al., 1997). Embryos were microinjected in 6% Ficoll in MMR 1× (100 mM NaCl, 2 mM KCl, 2 mM $MgCl_2$, 2.4 mM $CaCl_2$, 20 mM Hepes, pH 8.9) using a PLI-100 microinjector (Medical Systems Corp.). 10 nl (50 pg/blastomere) of plasmid DNA was microinjected into the animal pole of 4–8-cell stage embryos. After microinjections, embryos were reared at room temperature until they reached stage 7, when they were transferred in MMR 0.25× (25 mM NaCl, 0.5 mM KCl, 0.5 mM $MgCl_2$, 0.6 mM $CaCl_2$, 5 mM Hepes, pH 8.9) and allowed to develop at 15°C until the end of gastrulation.

Electron Microscopic Analysis of Purified Chicken Cingulin Rod

Cingulin was purified from chicken enterocytes and visualized by rotary shadowing electron microscopy as described previously (Citi et al., 1988). Purified chicken cingulin has an approximate size of M_r 108 kD, whereas anticingulin antisera recognize a polypeptide of M_r 140 kD in chicken epithelial cell lysate. This, and the observation that purified cingulin appears as a 130-nm-long rod, indicate that purified cingulin consists of only the coiled-coil region (and probably globular COOH-terminal tail), and is, thus, a proteolytic fragment of complete chicken cingulin (Citi et al., 1988, 1989). We refer here to purified chicken cingulin as cingulin rod. To test the ability of cingulin rod to aggregate, purified rod (1 mg/ml in 0.6 M NaCl, 10 mM NaH_2PO_4, pH 7.0, 1 mM DTT) was dialyzed at 4°C for 14 h against 50 mM sodium acetate, pH 5.0, 5 mM DTT. After dialysis, the

Published December 27, 1999

samples were stained with uranyl acetate and observed in the electron microscope as described (Hodge et al., 1992).

Northern Blotting

Total RNA was extracted from *Xenopus laevis* tissue using the Qiagen RNA extraction Midi Kit, and Northern blots were carried out as described in Cordenonsi et al. (1999). Digoxigenin-labeled nucleotidic probes were generated by PCR for cingulin using D902 as a template and primers forward 5′-AAGGAATTCATGGAAAGGGATATATATG-GCG-3′ and reverse 5′-GAGGAATTCACTCTGGACAGTTCTT-3′, and for actin using a rat muscle β-actin reverse transcriptase–PCR amplified fragment (nucleotide positions 218–822, provided by Dr. L. Dalla Valle, University of Padova, Padova, Italy) as a template and primers forward 5′-GAGCAAGAGAGGCATCCT-3′ and reverse 5′-GAAG-CAAGGCTGGAAGAG-3′.

SDS-PAGE, Immunoblotting, and Autoradiography

SDS-PAGE and immunoblotting were carried out as described in Cordenonsi et al. (1997). For autoradiography, gels were soaked for 30 min in fixing solution (40% methanol, 7% acetic acid), and for 30 min in Amplify solution (Amersham). They were dried onto blotting paper for 90 min at 80°C, and exposed at −70°C onto film for 14 to 62 h.

Immunofluorescence Microscopy

Whole mount immunofluorescence and observation of *Xenopus laevis* embryos was performed as described (Cordenonsi et al., 1997). MDCK cells were fixed with cold methanol and labeled as described (Citi, 1992). Labeled MDCK cells were observed with a Zeiss Axiovert S100TV microscope, using a 63× PlanApo (1.3 NA) objective. Images were acquired using a Hamamatsu C4742-95 CCD camera, controlled by Openlab image acquisition software, and digital images were processed with Adobe Photoshop 4.0 and Illustrator 8.0.

Results

Cingulin Contains a Globular Head, a Coiled-coil Rod, and a Globular Tail

A rabbit polyclonal antiserum (C532) against recombinant chicken cingulin was used to screen a phage expression library of *Xenopus laevis* ovary cDNA. An ~5.2-kb cDNA insert was identified, and its nucleotide sequence (5,191 bp) showed a 115-bp 5′ untranslated region, a 4,104-bp open reading frame, and a 972-bp 3′ untranslated region, which comprises a poly-A tail (Fig. 1). The open reading frame codes for a polypeptide of 1,368 amino acids, with a predicted size of 159,349 D, and a predicted pK_i of 5.61. The evidence that this clone effectively codes for *Xenopus laevis* cingulin is as follows: (1) the sequence of this clone is homologous (55% identical in the region of overlap) to the sequence of partial cDNAs of chicken cingulin, whose identity was in turn established based on sequence matches with tryptic peptides of purified chicken cingulin, and on the recognition of recombinant proteins by mAbs raised against purified native cingulin (Citi, 1994; Citi, S., and Kendrick-Jones, unpublished); (2) the predicted molecular size of the protein is very close to the estimated size of *Xenopus* embryo cingulin (M_r 160 kD) detected by immunoblotting of SDS-PAGE gels of embryo extracts (Cardellini et al., 1996); and (3) polyclonal antisera (M902 and R902) raised against a recombinant protein comprising the first 378 amino acids of the derived protein sequence (GST-XC(1-378), see Fig. 3 D) give immunofluorescent junctional staining in amphibian tissues (Cordenonsi et al., 1997; see Fig. 9) and recognize an M_r 160 kD protein in *Xenopus* embryo extracts (not shown).

To examine cingulin mRNA expression, total RNA from *Xenopus laevis* tissues was analyzed by Northern blot. A single band of ~5.4 kb was detected in the intestine (Fig. 2) and ovary tissue (not shown), indicating that only one cingulin message is present, and that our cDNA clone may lack ~200 bp of the untranslated region. The apparent lack of the cingulin message in fat bodies, a connective tissue (Fig. 2), is consistent with the idea that cingulin message is restricted to epithelial tissues, as predicted for a TJ protein.

The sequence of *Xenopus laevis* cingulin was analyzed to identify potentially significant motifs. A nuclear localization signal (PRGKRSK) is localized at residues 34–40 (Fig. 1), a potential helix-loop-helix dimerization domain at residues 190–198, and a leucine zipper at residues 1,003–1,024. Numerous potential serine phosphorylation sites are present in the sequence (5 for cAMP-dependent protein kinase, 31 for protein kinase C, and 33 for protein kinase CK2). There is also one potential tyrosine phosphorylation site (residues 214–221), but its significance is unclear, since in vivo phosphorylation has been detected only on serine residues (Citi and Denisenko, 1995). The hydrophobicity plot of *Xenopus laevis* cingulin indicates a hydrophylic protein, with no apparent membrane-spanning regions (Fig. 3 A). This is in agreement with previous data, indicating that cingulin is a cytoplasmic protein, based on extractability properties and immunoelectron microscopic localization (Citi et al., 1988, 1989).

Coiled-coil proteins are α-helical proteins showing heptad repeats of seven amino acid residues (*abcdefg*), where typically a and d are hydrophobic, and other residues are charged. Predicting the coiled-coil structure of *Xenopus laevis* cingulin indicates that the molecule consists of three regions (Fig. 3 B). First, an NH_2-terminal region of ~49 kD (439 amino acids, residues 1–439) with close to zero probability of coiled-coil, which is rich in serine residues and has pK_i of 9.06. Second, a central region of ~105 kD (886 amino acids, residues 440–1,325) with a very high probability of coiled-coil, which is rich in Glu, Leu, Lys, and Gln residues, and a pK_i of 5.21. Third, a short COOH-terminal region of ~4 kD (43 amino acids, residues 1,326–1,368) with close to zero probability of coiled coil, which is relatively rich in Ser residues and has a pK_i of 4.67. We refer to these regions as head, rod, and tail, respectively (Fig. 3 C). A trigger sequence motif (QRLEIELEESKE, residues 482–494) is located close to the proposed NH_2-terminal end of the coiled-coil rod domain. Such a motif may be necessary for the coiled-coil formation (Kammerer et al., 1998; Steinmetz et al., 1998).

Comparison of the derived amino acid sequence of the different regions of *Xenopus laevis* cingulin to sequences of other known proteins in sequence databases shows no significant homologies between the *Xenopus* cingulin head or tail sequences and known proteins, but significant homology to sequences in human and mouse EST databases (D'Atri, F., and S. Citi, manuscript in preparation). The cingulin rod sequence is homologous (20–22% identity and 40–44% similarity over stretches of up to 950 residues) to the rod portions of nonmuscle myosin II heavy chains, and, to a lesser extent, to other coiled-coil proteins.

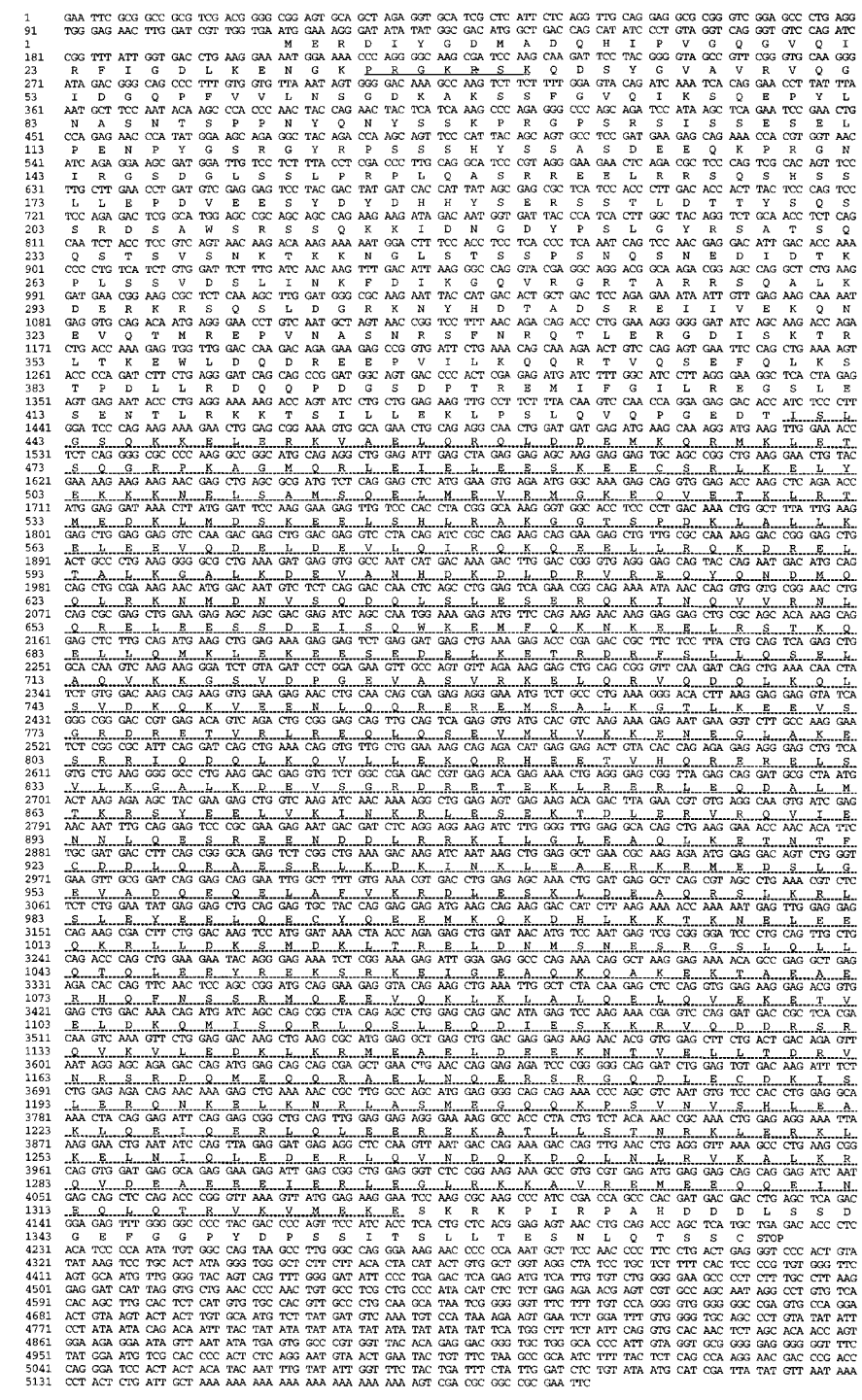

Figure 1. The nucleotide and derived amino acid sequence of *Xenopus laevis* cingulin. Single underline indicates nuclear localization sequence. Dashed underline indicates predicted coiled-coil sequence. The sequences are available from GenBank/EMBL/DDBJ under accession number AF207901.

The homologies of cingulin with the myosin heavy chain prompted us to further study the structure and properties of the coiled-coil region of cingulin.

Analysis of the Sequence and Assembly Properties of the Coiled-coil Region of Cingulin

The coiled-coil structure of almost all α-fibrous proteins contains discontinuities in the phasing of their underlying heptad substructure. Sometimes these correspond to quite long stretches of intervening sequence. Alternatively, the discontinuities may be shorter and contain one or more prolines or other residues that disrupt an α-helical conformation. More usually, the discontinuities are either stutters, stammers, or skips, which correspond to deletions of three or four residues, or insertion of one residue, respectively, in an otherwise continuous heptad repeat (Brown et al., 1996). Analysis of the sequence of the rod region of cingulin shows that the heptad repeats can be grouped in ten segments (residues 440–550, 556–608, 609–721, 724–783, 784–854, 855–1,034, 1,035–1,052, 1,053–1,210, 1,214–1,268, and 1,269–1,325). These are separated one from the

Published December 27, 1999

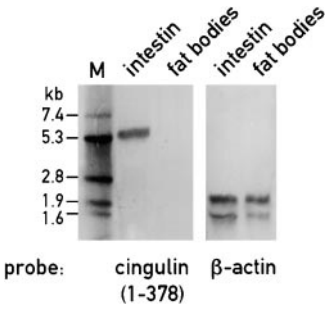

Figure 2. Northern blot analysis of *Xenopus* tissues total RNA, using cingulin and actin probes. An ~5.4-kb cingulin message is detected in intestine (epithelial tissue) but not in fat bodies (connective tissue). Numbers on the left indicate the migration of RNA size markers.

other by proline sequences (boundary between segments 1–2, 3–4, and 8–9), skip residues (segments 2–3, 4–5, and 5–6), and stutters (segments 6–7, 7–8, and 9–10). The α-helical content of the designated rod domain is 95–99%. Thus, there are no significant regions that do not conform to the coiled-coil structure. From the positions of residues within the heptad substructure there are key residue types that distinguish two- and three-stranded coiled coils. Analysis of these positions by the method of Woolfson and Alber (1995) shows that the two-stranded structure is strongly favored. The predicted length of the coiled-coil region of *Xenopus* cingulin is, thus, ~130 nm (886 residues × 0.1485 nm axial rise per residue). The coiled-coil structure of cingulin rod agrees with the biochemical data on the purified rod fragment of chicken cingulin, showing that it is a heat-stable dimer, with a fibrillar, rod-like shape, and a contour length of 130 nm (Citi et al., 1988, 1989). Furthermore, interchain ionic interactions between residues in specific positions of the heptad repeats in adjacent chains were calculated as a function of relative axial stagger (McLachlan and Stewart, 1975; Parry et al., 1977). The results give a score of +64 for a parallel in-register chain arrangement, corresponding to a highly significant value of 0.51 ionic interactions per heptad pair. Thus, we conclude that the coiled-coil region of cingulin is formed by two parallel chains arranged in axial register.

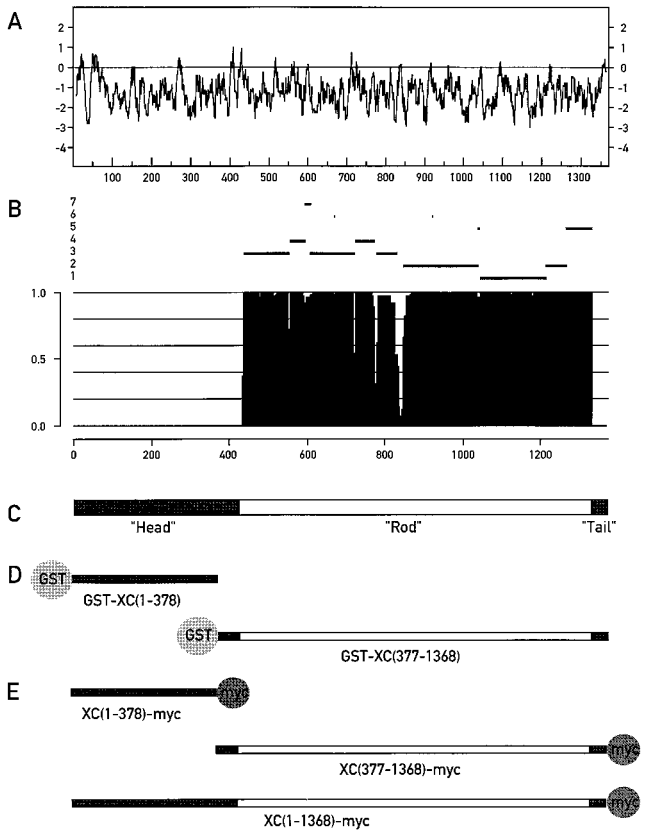

Figure 3. Structure predictions and domain organization of *Xenopus laevis* cingulin. (A) Kyte-Doolittle hydrophobicity plot of cingulin. Amino acid positions are indicated on the x-axis. (B) Coiled-coil prediction analysis of cingulin using the MacStripe program. A value of 1 indicates highest probability of coiled-coil. Horizontal lines above the plot indicate the seven frames of the heptad repeats. (C) A schematic domain organization of *Xenopus laevis* cingulin (see also Fig. 10). (D) Diagram of GST fusion protein constructs used in pull-down assays. (E) Diagram of Myc-tagged cingulin constructs used in transfection experiments.

To test whether the coiled-coil region of cingulin can assemble into higher order aggregates in vitro, purified chicken cingulin rod was dialyzed against a low salt solution at pH 5.0 and observed by negative staining electron microscopy. Cingulin rod (M_r 108 kD) appears by rotary shadowing-electron microscopy as an elongated protein of average length 130 nm (Fig. 4 A) (Citi et al., 1988). After dialysis, we observed the formation of individual filamentous aggregates (Fig. 4 B). No ordered paracrystals of cingulin rod were obtained using a variety of conditions, including presence of divalent cations, different pH, and presence of KCNS, which are known to favor the formation of paracrystals in certain coiled-coil proteins (Kendrick-Jones et al., 1969). The bends and kinks observed by electron microscopy in the coiled-coil region of cingulin rod (Citi et al., 1988) (Fig. 4 A) could be due to the stutters and skips in the sequence. An alternative explanation proposed by Brown et al. (1996) is that the stutters and skips lead to a local unwinding of the coiled-coil over a short axial distance.

We tested whether full-length cingulin is also capable of assembly via the rod, by producing it as a ^{35}S-labeled protein in a reticulocyte lysate system and examining its interaction with bacterially expressed fragments of *Xenopus* cingulin (Fig. 3 D) in a GST pull-down assay. Full-length cingulin interacted strongly with fusions of GST with a COOH-terminal fragment of cingulin (containing the coiled-coil rod region, the tail, and part of the NH_2-terminal globular region), weakly with a fusion comprising most of the NH_2-terminal globular region, and not at all with GST alone or with GST fused to a fragment of human ZO-1 (Fig. 5). This experiment indicated that full-length cingulin can interact effectively with a bacterially expressed protein consisting primarily of the rod region of cingulin.

Cingulin Interacts In Vitro with ZO-1, ZO-2, ZO-3, Myosin, and AF-6

To explore cingulin interaction with other TJ proteins and with myosin, GST fusion proteins comprising the NH_2-terminal and COOH-terminal fragments of cingulin (Fig. 3 D) were used for pull-down experiments from epithelial cell lysates. Immunoblot analysis of proteins bound to glutathione-Sepharose beads indicated that ZO-1, ZO-2, myosin, and AF-6 associated with the NH_2-terminal fragment

Published December 27, 1999

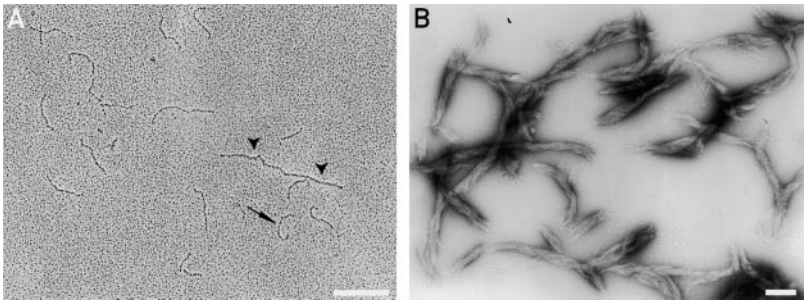

Figure 4. Electron microscopic analysis of purified chicken cingulin rod. (A) Rotary-shadowed molecules of cingulin rod. The arrow indicates one example of a 130-nm-long and 2-nm-wide molecule. The arrowheads indicate one example of an apparent cingulin oligomer. (B) Negatively stained twisted tangles of cingulin rod. The average length of the twisted tangles was 432 ± 51 nm (n = 36). Only isolated aggregates were scored. Bars, 150 nm.

of cingulin, and that myosin also associated with the COOH-terminal fragment of cingulin (Fig. 6 A). Symplekin was not found to associate either with the NH_2-terminal or the COOH-terminal cingulin fragments (Fig. 6 A).

To confirm the interactions of different fragments of cingulin with ZO-1, ZO-2, and myosin, and to further explore their interaction with ZO-3, GST-cingulin constructs were used to pull-down ^{35}S-labeled proteins produced in reticulocyte lysates (Fig. 6 B). ^{35}S-labeled ZO-1, ZO-2, ZO-3, and myosin interacted with the NH_2-terminal fragment of cingulin (Fig. 6 B). In addition, ^{35}S-labeled ZO-3 and myosin interacted with the COOH-terminal fragment of cingulin, although, especially in the case of ZO-3, the amount of labeled protein trapped by the COOH-terminal fragment of cingulin appeared considerably less than that trapped by the NH_2-terminal fragment (Fig. 6 B). These experiments suggested that cingulin interacts directly with ZO-1, ZO-2, ZO-3, and myosin.

To determine whether complexes of cingulin with ZO-1 and ZO-2 exist in vivo in epithelial cells, Triton-soluble and SDS-soluble fractions of cultured CaCo2 cells were immunoprecipitated either with anticingulin antiserum, or with anti–ZO-1 or anti–ZO-2 antibodies, and the immunoprecipitates were analyzed by Western blotting with anticingulin antiserum. Cingulin was detected in both the Triton-soluble and SDS-soluble pools of CaCo2 cells before and after immunoprecipitation (Fig. 6 C). After immunoprecipitation with anti–ZO-1 or anti–ZO-2 antibodies, cingulin was detected only in the SDS-soluble pool (Fig. 6 C), indicating the presence of a stable complex of cingulin with ZO-1 and ZO-2 in this pool, and suggesting that cytoskeletal interactions may stabilize the complex containing cingulin, ZO-1 and ZO-2 (see also Tsukamoto and Nigam, 1997). Conversely, ZO-1 or ZO-2 were not detected in cingulin immunoprecipitates (not shown), suggesting that only a fraction of ZO-1 and ZO-2 is complexed with cingulin in vivo.

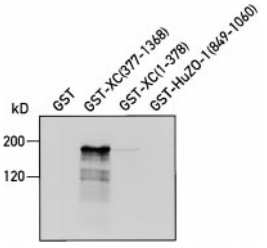

Figure 5. Self-interaction of *Xenopus laevis* cingulin. Radioactively labeled full-length cingulin, generated by in vitro transcription/translation, was detected by autoradiography after affinity purification on glutathione-Sepharose beads attached to GST, or GST-XC(377-1,368), GST-XC(1-378), or GST fused to a human ZO-1 fragment (amino acids 849–1,060) (GST-HuZO-1(849-1,060)). Strong association was detected with the COOH-terminal fragment of cingulin, no association with ZO-1 fragment or GST. Numbers on the left indicate approximate molecular sizes in kilodaltons, based on the migration of prestained markers.

To analyze quantitatively cingulin–ZO-1 interaction, lysates from ZO-1–infected Sf21 insect cells were used in pull-down assays with GST-XC(1-378). Immunoblot analysis with anti–ZO-1 antibodies revealed a major 220-kD polypeptide and several bands of smaller apparent size in infected Sf21 lysates (Fig. 7 A). After pull-down with GST-XC(1-378), only the 220-kD polypeptide was detected (Fig. 7 A). When a fixed amount of GST-XC(1-378) was incubated with increasing amounts of Sf21 cell lysate, the bound ZO-1 fraction was evaluated by Coomassie staining (Fig. 7 B). A plot of the data showed that the binding is saturable, and Scatchard analysis indicated a dissociation constant of ~5 nM (Fig. 7 C).

In Transfected MDCK Cells, Full-Length Cingulin Is Localized in Junctions, the NH_2-terminal Fragment Is Localized in the Nucleus and the Cytoplasm, and the COOH-terminal Fragment Is Localized in the Cytoplasm

We next used transfection with myc-tagged constructs (Fig. 3 E) to test whether full-length *Xenopus laevis* cingulin (residues 1–1,368), or the NH_2-terminal and COOH-terminal fragments used in the protein interaction experiments would be targeted to cell–cell junctions when transiently expressed in MDCK epithelial cells.

In mock-transfected cells, endogenous cingulin was localized along cell–cell junctions (Fig. 8 a), and no labeling was detected with the anti–tag mAb 9E10 (Fig. 8 a′). In cells transfected with full-length cingulin, the expressed protein was precisely colocalized with endogenous cingulin at sites of cell–cell contact (Fig. 8, b and b′). The transfected NH_2-terminal fragment was localized predominantly in the nucleus (Fig. 8, c and c′) and occasionally in the cytoplasm (Fig. 8, d and d′) but not in the junctional regions. Transfected COOH-terminal fragment accumulated in the cytoplasm either in a diffuse pattern (Fig. 8 e′) or in the form of large aggregates (Fig. 8 f′). Endogenous cingulin appeared normally localized in the junctional regions (Fig. 8, e and f). The presence of brightly stained aggregates could be due to aggregation or polymerization, possibly as a result of overexpression.

In Microinjected Xenopus laevis Embryos, the NH_2-terminal Fragment of Cingulin Is Localized in the Nucleus and in the Cytoplasm, and the COOH-terminal Fragment Is Localized in the Cytoplasm

To study the intracellular distribution of the NH_2-terminal and COOH-terminal fragments of *Xenopus laevis* cingulin

Published December 27, 1999

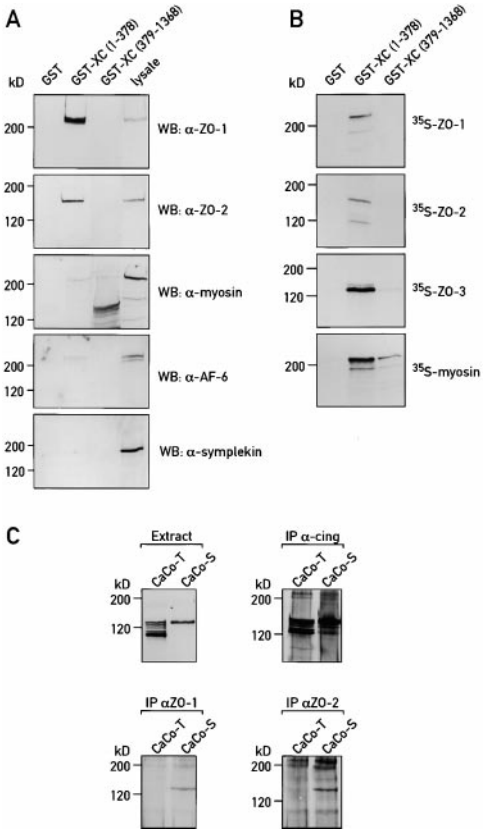

Figure 6. Interaction of cingulin with ZO-1, ZO-2, ZO-3, myosin, AF-6, and symplekin. (A) GST pull-downs from epithelial cell lysates using bacterially expressed cingulin. Western blots of MDCK cell lysates after affinity purification on glutathione-Sepharose beads attached to GST, GST-XC(1-378), or GST-XC(377-1,368), or before affinity purification (lysate). ZO-1, ZO-2, and AF-6 appear to associate only with cingulin NH_2-terminal fragment, myosin associates with both NH_2-terminal and COOH-terminal fragments, and symplekin does not associate with any fragment. (B) GST pull-downs from reticulocyte lysates containing radioactively labeled in vitro translated proteins. Autoradiography of ^{35}S-labeled ZO-1, ZO-2, ZO-3, and myosin, after affinity purification on glutathione-Sepharose beads attached to GST (GST), GST fusions of *Xenopus* cingulin NH_2-terminal fragment (GST-XC(1-378)), or COOH-terminal fragment (GST-XC(377-1,368)). ZO-1 and ZO-2 associate only with the NH_2-terminal fragment, ZO-3 and myosin associate with both NH_2-terminal and COOH-terminal fragments. (C) Coimmunoprecipitation of cingulin with ZO-1 and ZO-2. Western blot analysis, using anti-cingulin antiserum C532, of cingulin in Triton-soluble (CaCo-T) and SDS-soluble (CaCo-S) fractions of human CaCo2 cultured epithelial cells. (top left) Cell extract; (top right) extract after immunoprecipitation with anticingulin antiserum (IP α-cing); (bottom left) extract after immunoprecipitation with anti–ZO-1 antibodies (IP αZO-1); and (bottom right) extract after immunoprecipitation with anti–ZO-2 antibodies (IP αZO-2). Cingulin (M_r 140 kD) is detected in ZO-1 and ZO-2 immunoprecipitates from the SDS-soluble fraction. Polypeptides of M_r 100–135 kD detected in the Triton-soluble fraction of CaCo2 lysates probably represent proteolytic degradation products.

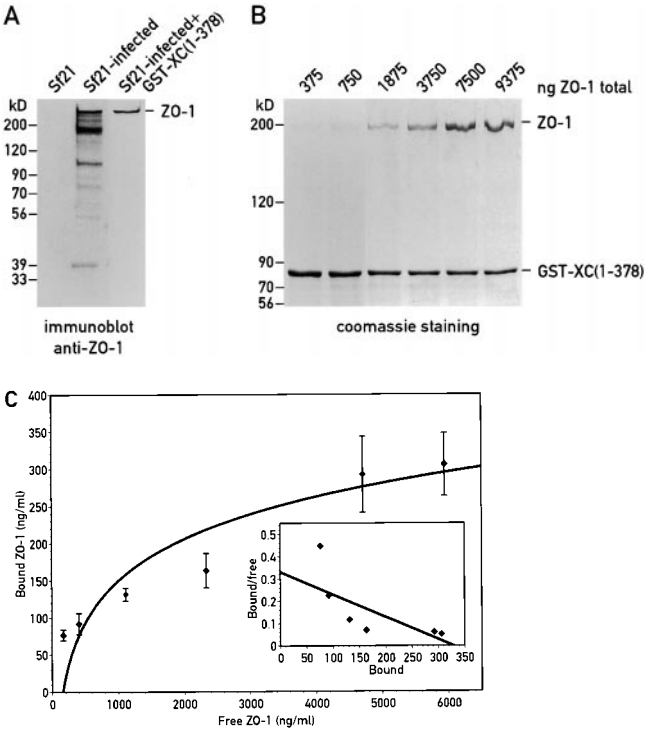

Figure 7. Quantitative analysis of the interaction between mouse ZO-1 and cingulin NH_2-terminal fragment. (A) Immunoblot analysis with anti–ZO-1 mAb R40.76 of lysates of control Sf21 cells, lysates of Sf21 cells infected with mouse ZO-1 baculovirus, and the same lysates after affinity purification on glutathione-Sepharose beads attached to GST-XC(1-378). (B) Coomassie-stained gel showing the bound fraction when increasing amounts of Sf21 lysates (numbers on top indicate ng total ZO-1 presentin lysate) were incubated with 2.5 μg GST-XC(1-378) attached to glutathione-Sepharose. (C) Plot showing the amount of ZO-1 bound as a function of free (total minus bound) ZO-1 in the Sf21 lysate, and Scatchard plot analysis of the same data (inset). Each point is the mean of two distinct experiments. The amounts of total ZO-1 in the lysate, and the bound fraction were measured as described in Materials and Methods. The binding was saturable, and the estimated dissociation constant was ~5 nM.

in epithelial cells of the same species, early *Xenopus* embryos were microinjected with constructs in the vector pCS2. Using this system, proteins are not expressed until transcription of the zygotic genome occurs, around mid-blastula transition. Thus, protein expression is detected only in cells that have inherited sufficient plasmid after repeated division of the microinjected blastomeres.

In control embryos, endogenous cingulin was localized along cell–cell junctions, and no labeling was detected with the anti–Myc antibody (Fig. 9, a and a′). In embryos microinjected with a Myc-tagged construct of the COOH-terminal fragment of cingulin, transfected protein accumulated in a diffuse form in cytoplasm and was absent from the nucleus (Fig. 9 b′). The absence of aggregates, which were detected in transfected MDCK cells (Fig. 8, f and f′), may depend on lower expression levels in embryos.

Embryos microinjected with a nontagged construct of the NH_2-terminal fragment of cingulin were stained with a polyclonal antiserum (R902) against the NH_2-terminal fragment of cingulin. This allowed detection of both endogenous and transfected cingulin in the same blastomeres. Analysis of embryos in an apical plane of focus (corresponding to TJ) showed junctional labeling of cingu-

Published December 27, 1999

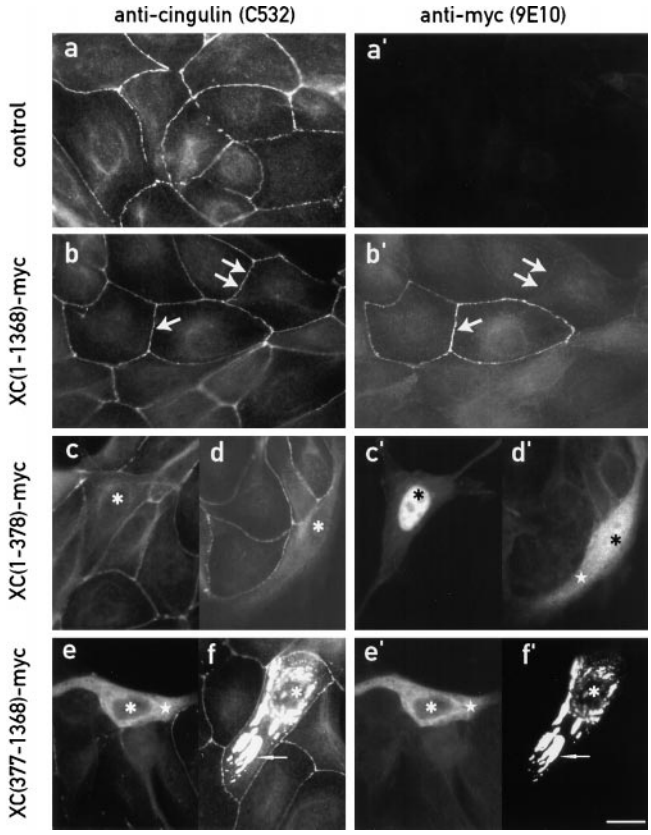

Figure 8. Localization of cingulin in transiently transfected MDCK cells. Double immunofluorescent staining of mock-transfected MDCK cells (a and a′), or MDCK cells transfected with XC(1-1,368)-myc (b and b′), or with XC(1-378)–myc (c, c′, d, and d′), or with XC(377-1,368)-myc (e, e′, f, and f′), using anticingulin antiserum C532 followed by TRITC anti-rabbit (a–f) and anti–myc 9E10 antibody followed by FITC anti-mouse (a′–f′). C532 labels endogenous cingulin and transfected cingulin when the COOH-terminal fragment is present in the transfection construct. 9E10 labels expressed cingulin. Mock-transfected cells were transfected with solvent or with vector alone. Single arrow in b (corresponding arrow in b′) indicates colocalization of endogenous and transfected cingulin in the junctional region between two cells. Double arrows in b and b′ indicate a junction containing endogenous cingulin but not transfected cingulin. Asterisks in c–f (corresponding asterisks in c′–f′) indicate nuclear regions. Asterisks in d′ and in e and e′ indicate cytoplasmic labeling of transfected protein. Thin arrows in f and f′ indicate brightly stained cytoplasmic aggregates. Bar, 10 μm.

lin both in expressing and nonexpressing blastomeres (Fig. 9 c). In addition, unlike surrounding cells, expressing blastomeres showed abundant cytoplasmic labeling (Fig. 9 c, star). Analysis of the same embryo in a more basal plane of focus showed no cingulin labeling in nonexpressing blastomeres and cytoplasmic and nuclear labeling in expressing blastomeres (Fig. 9 d). Some cingulin staining could also be detected near the cell periphery in expressing blastomeres. In summary, the cytoplasmic localization of the COOH-terminal fragment of cingulin and the nuclear and cytoplasmic localization of the NH_2-terminal fragment of cingulin were consistently observed in transfected or microinjected cells from different species.

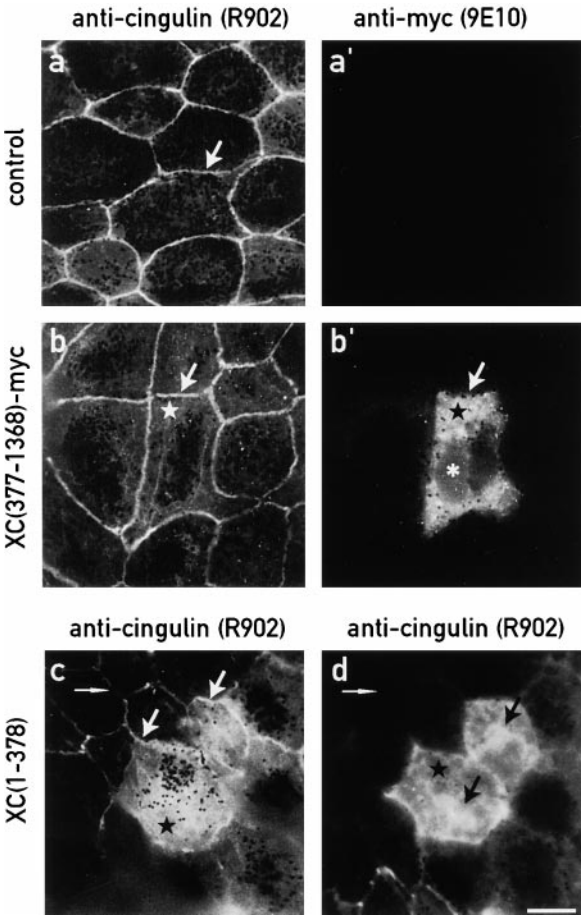

Figure 9. Localization of cingulin in *Xenopus laevis* embryos (gastrula stage) after microinjection of early embryos with cingulin constructs in pCS2. Double immunofluorescent staining of mock-microinjected embryos (a and a′), or embryos microinjected with XC(377-1,368)-myc in pCS2 (b and b′), using anticingulin antiserum R902 followed by FITC anti-rabbit (a and b) and 9E10 antibody followed by TRITC anti-mouse (a′ and b′). Arrows in a and b (corresponding arrow in b′) indicate junctional cingulin immunolabeling. Star in b′ (corresponding star in b) indicates cytoplasmic labeling of transfected protein. Asterisk in b′ indicates nuclear region. Note that XC(377-1,368)–myc is distributed in the cytoplasm and absent from junctions and nuclear regions. c and d show two different focal planes (c, apical; d, subapical) of an embryo that was microinjected with residues 1–378 of cingulin without Myc tag (XC(1-378)) and stained with anticingulin antiserum R902 followed by TRITC-anti-rabbit. R902 antiserum was raised against the NH_2-terminal region of cingulin (Cordenonsi et al., 1997), and recognizes both endogenous and transfected cingulin. White arrows in c indicate apical junctional cingulin staining in two adjacent blastomeres. Black arrows in d indicate nuclear regions in a lower plane of focus in the same blastomeres shown in c. Black star in d indicates cytoplasm. Black dots visible in b′ and c against the light background represent pigment granules. Bar, 20 μm.

Discussion

Cingulin Structure and Implications for Its Function

Cingulin is an M_r 140–160-kD protein originally identified as a peripheral component of epithelial TJ (Citi et al., 1988). Although its expression in different tissues and spe-

Published December 27, 1999

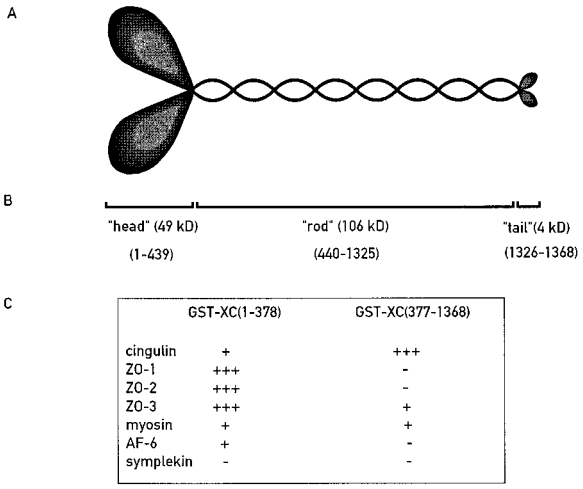

	GST-XC(1-378)	GST-XC(377-1368)
cingulin	+	+++
ZO-1	+++	-
ZO-2	+++	-
ZO-3	+++	+
myosin	+	+
AF-6	+	-
symplekin	-	-

Figure 10. (A) A schematic cartoon showing the putative organization of cingulin as a parallel dimer with globular and coiled-coil domains. (B) Proposed names, sizes, and amino acid boundaries of different *Xenopus* cingulin regions. (C) Summary of in vitro interactions of GST fusion proteins of NH_2-terminal (1–378) and COOH-terminal (377–1,368) fragments of *Xenopus* cingulin. Positive score indicates interaction detected (with number of + proportional to relative intensities of signal using different approaches), a negative score indicates interaction not detected.

cies and its subcellular localization under various experimental conditions have been characterized in some detail (Citi, 1994), its molecular structure was so far unknown. We now show data indicating that cingulin is a parallel dimer of two subunits, each with a globular head, a coiled-coil rod, and a globular tail (Fig. 10, A and B). This organization is reminiscent of conventional myosins. However, the globular region of cingulin is smaller than that of myosins (49 versus 80 kD), and, unlike myosins, the sequence of the globular NH_2-terminal region of cingulin does not reveal obvious actin- or ATP-binding motifs. Hence, it seems unlikely that the cingulin head could behave as a myosin-like motor domain, capable of generating mechanical tension via an ATP-dependent interaction with actin. While further experiments are in progress to investigate the actin-binding and enzymatic activities of cingulin, present data indicate that the cingulin head is primarily involved in interactions with other proteins (Fig. 10 C), and the cingulin rod is involved primarily in dimerization (possibly higher order assembly) and interaction with myosin. Although it is unclear whether cingulin actually self-assembles in vivo, the ability of cingulin to form polymers could potentially provide a structural scaffold and organizing web on the cytoplasmic face of TJ. For example, cingulin polymers may serve to cross-link different areas of the junction by interaction with TJ proteins and the cytoskeleton (see below).

Cingulin Interacts with TJ Proteins and Myosin: A Link between TJ and the Cytoskeleton?

Using different in vitro experimental approaches (GST pull-down from lysates of epithelial insect cells and reticulocytes) we showed that cingulin interacts in vitro with some of the known protein constituents of TJ, namely ZO-1, ZO-2, and ZO-3, and with AF-6 and myosin. An in vivo interaction of cingulin with ZO-1 and ZO-2 is suggested by the presence of cingulin in ZO-1 and ZO-2 immunoprecipitates. In addition, cingulin interacts in vitro with occludin (Cordenonsi et al., 1999) and JAM (Bazzoni, G., O.M. Martinez-Estrada, M. Cordenonsi, S. Citi, and E. Dejana, manuscript submitted for publication). Thus, we propose that cingulin is a key component of the multiprotein complex on the cytoplasmic face of the TJ.

Cingulin was found to associate with human, canine, and mouse ZO-1, human and canine ZO-2, canine ZO-3, and canine AF-6. All of these proteins have been localized in TJ in epithelial cells (Stevenson et al., 1986; Jesaitis and Goodenough, 1994; Yamamoto et al., 1997; Haskins et al., 1998), even though ZO-1 and ZO-2 are also localized at adherens-type junctions in nonepithelial cells (Itoh et al., 1991, 1999; Howarth et al., 1992) and the localization of AF-6 in TJ versus zonula adherens is controversial (Mandai et al., 1997; Yamamoto et al., 1997; Zhadanov et al., 1999). Since cingulin appears to be exclusively localized in TJ of epithelial cells (Citi et al., 1988, 1989), it seems likely that such interactions are physiologically relevant. In addition, the estimated dissociation constant ($\sim$5 nM) for cingulin–ZO-1 interaction (Fig. 7) is sufficiently small to suggest that direct interaction with ZO-1 can occur in vivo. On the other hand, since the amount of AF-6 pulled down by cingulin appeared small (Fig. 6 A), it is possible that this interaction is not direct, but is mediated by other proteins, for example ZO-1.

The interaction of cingulin with myosin (Fig. 6) is consistent with the previous observation that cingulin copurifies with myosin from intestinal brush border cells (Citi et al., 1989) and is disrupted by increasing NaCl concentration (D'Atri, F., and S. Citi, unpublished observations), suggesting that intermolecular ionic interactions between the coiled-coil regions may play a role. What could be the physiological significance of cingulin interaction with myosin? Drugs and signaling proteins that control the assembly and contractility of the actomyosin cytoskeleton, including small GTP-binding proteins and myosin light chain kinase, can affect dramatically TJ assembly, structure, and function (Madara et al., 1987; Citi et al., 1994; Turner et al., 1997; Jou et al., 1998), leading to the hypothesis that purse-string contraction of the circumferential actomyosin belt localized at the level of the zonula adherens can modulate the degree of sealing and, thus, the barrier function of TJ (Citi and Cordenonsi, 1998; Fanning et al., 1998). Modulation of TJ function by contraction of subcortical actomyosin may occur by direct interaction of TJ proteins with components of the TJ actomyosin cytoskeleton. Such a role could be played by ZO-1, which is so far the only TJ protein reported to bind to actin (Itoh et al., 1997; Fanning et al., 1998). However, our data indicate that cingulin could also be involved. Cingulin interaction with myosin might serve to transduce the mechanical force generated by the contraction of the actomyosin cytoskeleton to proteins of the cytoplasmic plaque and membrane domains of TJ. In addition, since cingulin is so far the only TJ protein detected in an apical cortical localization in early embryos (Fleming et al., 1993; Cardellini et al., 1996), its interaction with the actomyosin cytoskeleton may be re-

Published December 27, 1999

lated to the establishment of structural asymmetry in the plasma membrane (Yeaman et al., 1999), in vertebrate development, and in its maintenance in adult tissues.

It is now clear that most TJ proteins associate in vitro with a multitude of protein partners. For example, ZO-1 interacts in vitro with the cytoplasmic regions of membrane proteins, such as occludin (Furuse et al., 1994; Fanning et al., 1998), connexin (Giepmans and Moolenaar, 1998; Toyofuku et al., 1998), and JAM (Bazzoni, G., O.M. Martinez-Estrada, M. Cordenonsi, S. Citi, and E. Dejana, manuscript submitted for publication), with PDZ proteins, such as ZO-2 (Gumbiner et al., 1991), p130/ZO-3 (Balda et al., 1993; Haskins et al., 1998), AF-6 (Yamamoto et al., 1997, 1999), and canoe (Takahashi et al., 1998), with the protein kinase ZAK (Balda et al., 1996), and with cytoskeletal proteins such as catenins (Rajasekaran et al., 1996; Itoh et al., 1997), cortactin (Katsube et al., 1998), actin (Itoh et al., 1997; Fanning et al., 1998), and fodrin/spectrin (Itoh et al., 1991; Tsukamoto and Nigam, 1997). ZO-2 interacts with occludin and α-catenin (Itoh et al., 1999), and ZO-3 interacts with occludin and ZO-1 but not with ZO-2 (Haskins et al., 1998). To determine the physiological relevance of all these interactions, as well as the newly identified interactions of cingulin with other junctional and cytoskeletal proteins, it will be important to establish hierarchies of binding, based on the measurement of dissociation constants in vitro, and to examine the molecular organization of TJ in vivo in cells and organisms lacking specific TJ components.

Cingulin Localization in Transfected Cells: In Vivo Interactions of the NH_2-terminal and COOH-terminal Fragments of Cingulin

Transfection experiments in MDCK cells showed that TJ targeting of expressed cingulin occurred only with the full-length sequence, but not with the NH_2-terminal or COOH-terminal fragments alone. Thus, sequences in both the NH_2-terminal and COOH-terminal regions of cingulin are required for correct targeting to TJ. Based on the protein interactions data, we hypothesize that the TJ targeting of the full-length *Xenopus* cingulin in transfected MDCK cells depends primarily on sequences in the cingulin head, which associate with several TJ proteins in vitro (Figs. 6 and 10), whereas the cingulin rod associates weakly only with ZO-3.

The observation that the NH_2-terminal fragment alone was not targeted to TJ was unexpected, since protein interaction experiments indicated that this fragment associates with several TJ proteins in vitro (Fig. 6). Since a similar localization was obtained in transfected MDCK cells and in microinjected *Xenopus* embryos, the nuclear/cytoplasmic localization was not related to species-specific differences in the amphibian and canine cingulin sequences. Why does the NH_2-terminal globular region of cingulin require the COOH-terminal region to be targeted to TJ? One possibility is that the COOH-terminal region allows the NH_2-terminal part of the molecule to fold into an optimal conformation or bind to specific sorting machineries. Second, cingulin may have to form coiled-coil dimers or assemble into supramolecular aggregates to be targeted or sorted to the junction, and specific parts of the coiled-coil region may be required for dimerization and multimerization. On the other hand, the observation that the COOH-terminal fragment, comprising all of the coiled-coil region plus a small part of the globular head, does not target to TJ, and shows that the potential for dimerization or multimerization is not sufficient for TJ targeting. Although this fragment associates with cingulin and weakly with ZO-3 in vitro, these interactions may not be favored in vivo, or not be sufficient to target the fragment to TJ. Taken together, all these observations indicate that sequences in the head region are critical for TJ targeting, presumably because of their interaction with specific TJ proteins, but additional sequences in the rod are important. The identity of these sequences is currently being investigated. The nuclear localization of the transfected NH_2-terminal fragment could be due to passive diffusion of the mistargeted protein through the lateral channels of the nuclear pore complex (Paine, 1975), or due to some affinity of cingulin NH_2-terminal fragment for nuclear proteins. Interestingly, endogenous cingulin can be localized in the nucleus in subconfluent cultured MDCK cells (Citi and Cordenonsi, 1999).

We report here the first structure/function analysis in vitro of the TJ protein cingulin, and show that cingulin contains distinct structural domains responsible for self-assembly and interaction with other TJ proteins and myosin. These and other data (Cordenonsi et al., 1999; Bazzoni, G., O.M. Martinez-Estrada, M. Cordenonsi, S. Citi, and E. Dejana, manuscript submitted for publication) allow us to propose that cingulin is a functionally important component of the multiprotein complex on the cytoplasmic face of TJ. Cingulin may contribute to TJ physiology by forming a scaffolding web on the cytoplasmic face of TJ, and a link between the TJ plaque and the cytoskeleton. To obtain more direct information on the role of cingulin in TJ physiology, studies on cingulin are being pursued by biochemical, cell biological, and molecular approaches.

We are indebted to all the colleagues who generously provided us with reagents: R. Adelstein, J. Anderson, G. Evan, D. Goodenough, M. Itoh, A. LeBivic, K. Simons, and B. Stevenson. We also thank S. Edelstein, N. Roggli, and T. Hodge for advice, support, and assistance.

This work was supported by Ministero dell' Universitá della Ricerca Scientifica e Tecnologia, Consiglio Nationale delle Ricerca, European Union, Biomed Programme (BMH4CT950090), Swiss National Fonds, and the Canton of Geneva.

Submitted: 3 August 1999
Revised: 8 November 1999
Accepted: 12 November 1999

References

Balda, M.S., L. Gonzalez-Mariscal, K. Matter, M. Cereijdo, and J.M. Anderson. 1993. Assembly of the tight junction: the role of diacylglycerol. *J. Cell Biol.* 123:293–302.

Balda, M.S., J.M. Anderson, and K. Matter. 1996. The SH3 domain of the tight junction protein ZO-1 binds to a serine protein kinase that phosphorylates a region C-terminal to this domain. *FEBS (Fed. Eur. Biochem. Soc.) Lett.* 399: 326–332.

Beatch, M., L.A. Jesaitis, W.J. Gallin, D.A. Goodenough, and B.R. Stevenson. 1996. The tight junction protein ZO-2 contains three PDZ (PSD-95/Discs-Large/ZO-1) domains and an alternatively spliced region. *J. Biol. Chem.* 271: 25723–25726.

Brown, J.H., C. Cohen, and D.A.D. Parry. 1996. Heptad breaks in alpha-helical coiled coils: stutters and stammers. *Proteins.* 26:134–145.

Cardellini, P., G. Davanzo, and S. Citi. 1996. Tight junctions in early amphibian development: detection of junctional cingulin from the 2-cell stage and its localization at the boundary of distinct membrane domains in dividing blastomeres in low calcium. *Dev. Dyn.* 207:104–113.

Chou, P.Y., and G.D. Fasman. 1978. Prediction of the secondary structure of proteins from their amino acid sequence. *Adv. Enzymol. Relat. Areas Mol. Biol.* 47:45–148.

Citi, S. 1992. Protein kinase inhibitors prevent junction dissociation induced by low extracellular calcium in MDCK epithelial cells. *J. Cell Biol.* 117:169–178.

Citi, S. 1994. The molecular composition of tight junctions. *In* Molecular Mechanisms of Epithelial Cell Junctions: From Development to Disease. S. Citi, editor. R.G. Landes, Austin, TX. 83–106.

Citi, S., and J. Kendrick-Jones. 1987. Studies on the structure and conformation of brush border myosin using monoclonal antibodies. *Eur. J. Biochem*. 165: 315–325.

Citi, S., and N. Denisenko. 1995. Phosphorylation of the tight junction protein cingulin and the effect of protein kinase inhibitors and activators in MDCK epithelial cells. *J. Cell Sci.* 108:2917–2926.

Citi, S., and M. Cordenonsi. 1998. Tight junction proteins. *Biochim. Biophys. Acta.* 1448:1–11.

Citi, S., and M. Cordenonsi. 1999. The molecular basis for the structure, function and regulation of tight junctions. *In* Adhesive Interactions of Cells. Vol. 28. D.R. Garrod, A.J. North, and M.A.J. Chidgey, editors. JAI Press, Inc., Greenwich, CT. 203–233.

Citi, S., H. Sabanay, R. Jakes, B. Geiger, and J. Kendrick-Jones. 1988. Cingulin, a new peripheral component of tight junctions. *Nature.* 333:272–276.

Citi, S., H. Sabanay, J. Kendrick-Jones, and B. Geiger. 1989. Cingulin: characterization and localization. *J. Cell Sci.* 93:107–122.

Citi, S., T. Volberg, A.D. Bershadsky, N. Denisenko, and B. Geiger. 1994. Cytoskeletal involvement in the modulation of cell-cell junctions by the protein kinase inhibitor H-7. *J. Cell Sci.* 107:683–692.

Cordenonsi, M., E. Mazzon, L. De Rigo, S. Baraldo, F. Meggio, and S. Citi. 1997. Occludin is dephosphorylated in the early stages of *Xenopus laevis* development. *J. Cell Sci.* 110:3131–3139.

Cordenonsi, M., F. Turco, F. D'Atri, E. Hammar, G. Martinucci, F. Meggio, and S. Citi. 1999. *Xenopus laevis* occludin: identification of in vitro phosphorylation sites by protein kinase CK2 and association with cingulin. *Eur. J. Biochem*. 264:374–384.

De Boer, A.G., and D.D. Breimer. 1994. The blood-brain barrier: clinical implications for drug delivery to the brain. *J. R. Coll. Physicians Lond.* 28:502–506.

Fanning, A.S., B.J. Jameson, L.A. Jesaitis, and J.M. Anderson. 1998. The tight junction protein ZO-1 establishes a link between the transmembrane protein occludin and the actin cytoskeleton. *J. Biol. Chem*. 273:29745–29753.

Farquhar, M.G., and G.E. Palade. 1963. Junctional complexes in various epithelia. *J. Cell Biol.* 17:375–412.

Fleming, T.P., M. Hay, Q. Javed, and S. Citi. 1993. Localisation of tight junction protein cingulin is temporally and spatially regulated during early mouse development. *Development.* 117:1135–1144.

Furuse, M., T. Hirase, M. Itoh, A. Nagafuchi, S. Yonemura, S. Tsukita, and S. Tsukita. 1993. Occludin: a novel integral membrane protein localizing at tight junctions. *J. Cell Biol.* 123:1777–1788.

Furuse, M., M. Itoh, T. Hirase, A. Nagafuchi, S. Yonemura, S. Tsukita, and S. Tsukita. 1994. Direct association of occludin with ZO-1 and its possible involvement in the localization of occludin at tight junctions. *J. Cell Biol.* 127: 1617–1626.

Furuse, M., K. Fujita, T. Hiiragi, K. Fujimoto, and S. Tsukita. 1998. Claudin-1 and -2: novel integral membrane proteins localizing at tight junctions with no sequence similarity to occludin. *J. Cell Biol*. 141:1539–1550.

Garnier, J., D.J. Osguthorpe, and B. Robson. 1978. Analysis of the accuracy and implications of simple methods for predicting the secondary structure of globular proteins. *J. Mol Biol*. 120:97–120.

Giepmans, B.N., and W.H. Moolenaar. 1998. The gap junction protein connexin-43 interacts with the second PDZ domain of the zona occludens-1 protein. *Curr. Biol*. 8:931–934.

Graham, F.L., and A.J. van der Eb. 1973. Transformation of rat cells by DNA of human adenovirus 5. *Virology*. 54:536–539.

Gumbiner, B., T. Lowenkopf, and D. Apatira. 1991. Identification of a 160 kDa polypeptide that binds to the tight junction protein ZO-1. *Proc. Natl. Acad. Sci. USA*. 88:3460–3464.

Haskins, J., L. Gu, E.S. Wittchen, J. Hibbard, and B.R. Stevenson. 1998. ZO-3, a novel member of the MAGUK protein family found at the tight junction, interacts with ZO-1 and occludin. *J. Cell Biol*. 141:199–208.

Hodge, T.P., R. Cross, and J. Kendrick-Jones. 1992. Role of the COOH-terminal nonhelical tailpiece in the assembly of a vertebrate nonmuscle myosin rod. *J. Cell Biol*. 118:1085–1095.

Howarth, A.G., M.R. Hughes, and B.R. Stevenson. 1992. Detection of the tight junction-associated protein ZO-1 in astrocytes and other nonepithelial cell types. *Am. J. Physiol.* 262:C461–C469.

Itoh, M., S. Yonemura, A. Nagafuchi, S. Tsukita, and S. Tsukita. 1991. A 220-kD undercoat-constitutive protein: its specific localization at cadherin-based cell–cell adhesion sites. *J. Cell Biol.* 115:1449–1462.

Itoh, M., A. Nagafuchi, S. Yonemura, T. Yasuda-Kitani, S. Tsukita, and S. Tsukita. 1993. The 220-kD protein colocalizing with cadherins in nonepithelial cells is identical to ZO-1, a tight junction–associated protein in epithelial cells: cDNA cloning and immunoelectron microscopy. *J. Cell Biol.* 121:491–502.

Itoh, M., A. Nagafuchi, S. Moroi, and S. Tsukita. 1997. Involvement of ZO-1 in cadherin-based cell adhesion through its direct binding to α-catenin and actin filaments. *J. Cell Biol*. 138:181–192.

Itoh, M., K. Morita, and S. Tsukita. 1999. Characterization of ZO-2 as a MAGUK family member associated with tight as well as adherens junctions with a binding affinity to occludin and alpha catenin. *J. Biol. Chem*. 274: 5981–5986.

Jesaitis, L.A., and D.A. Goodenough. 1994. Molecular characterization and tissue distribution of ZO-2, a tight junction protein homologous to ZO-1 and the *Drosophila* discs-large tumor suppressor protein. *J. Cell Biol.* 124:949–961.

Jou, T.S., E.E. Schneeberger, and W.J. Nelson. 1998. Structural and functional regulation of tight junctions by RhoA and Rac1 small GTPases. *J. Cell Biol*. 142:101–115.

Kammerer, R.A., T. Schulthess, R. Landwehr, A. Lustig, J. Engel, U. Aebi, and M.O. Steinmetz. 1998. An autonomous folding unit mediates the assembly of two-stranded coiled coils. *Proc. Natl. Acad. Sci. USA*. 95:13419–13424.

Katsube, T., M. Takahisa, R. Ueda, N. Hashimoto, M. Kobayashi, and S. Togashi. 1998. Cortactin associates with the cell-cell junction protein ZO-1 in both *Drosophila* and mouse. *J. Biol. Chem*. 273:29672–29677.

Kendrick-Jones, J., C. Cohen, A.G. Szent-Gyorgyi, and W. Longley. 1969. Paramyosin: molecular length and assembly. *Science*. 163:1196–1198.

Keon, B.H., S. Schafer, C. Kuhn, C. Grund, and W.W. Franke. 1996. Symplekin, a novel type of tight junction plaque protein. *J. Cell Biol.* 134:1003–1018.

Knight, A.E. 1994. The Diversity of Myosin-Like Proteins. Ph.D. thesis. University of Cambridge, Cambridge, UK. 254 pp.

Madara, J.L., R. Moore, and S. Carlson. 1987. Alteration of intestinal tight junction structure and permeability by cytoskeletal contraction. *Am. J. Physiol.* 253:C854–C861.

Mandai, K., H. Nakanishi, A. Satoh, H. Obaishi, M. Wada, H. Nishioka, M. Itoh, A. Mizoguchi, T. Aoki, T. Fujimoto, et al. 1997. Afadin: a novel actin filament-binding protein with one PDZ domain localized at cadherin-based cell-to-cell adherens junction. *J. Cell Biol*. 139:517–528.

Martin-Padura, I., S. Lostaglio, M. Schneemann, L. Williams, M. Romano, P. Fruscella, C. Panzeri, A. Stoppacciaro, L. Ruco, A. Villa, D. Simmons, and E. Dejana. 1998. Junctional adhesion molecule, a novel member of the immunoglobulin superfamily that distributes at intercellular junctions and modulates monocyte transmigration. *J. Cell Biol*. 142:117–127.

McLachlan, A.D., and M. Stewart. 1975. Tropomyosin coiled-coil interactions: evidence for an unstaggered structure. *J. Mol. Biol.* 98:293–304.

Mitic, L.L., and J.M. Anderson. 1998. Molecular architecture of tight junctions. *Annu. Rev. Physiol.* 60:121–142.

Paine, P.L. 1975. Nucleocytoplasmic movement of fluorescent tracers microinjected into living salivary gland cells. *J. Cell Biol.* 66:652–657.

Parry, D.A.D., W.G. Crewther, R.D.B. Fraser, and T.P. MacRae. 1977. Structure of alpha-keratin: structural implication of the amino acid sequences of the type I and type II chain segments. *J. Mol. Biol.* 113:449–454.

Prasad, R., Y. Gu, H. Alder, T. Nakamura, O. Canaani, H. Saito, K. Huebner, R.P. Gale, P.C. Nowell, K. Kuriyama, et al. 1993. Cloning of the ALL-1 fusion partner, the AF-6 gene, involved inacute myeloid leukemias with the t(6;11) chromosome translocation. *Cancer Res.* 53:5624–5628.

Rajasekaran, A.K., M. Hojo, T. Huima, and E. Rodriguez-Boulan. 1996. Catenins and zonula occludens-1 form a complex during early stages in the assembly of tight junctions. *J. Cell Biol*. 132:451–463.

Rupp, R.A., L. Snider, and H. Weintraub. 1994. *Xenopus* embryos regulate the nuclear localization of XMyoD. *Genes Dev*. 8:1311–1323.

Saitou, M., K. Fujimoto, Y. Doi, M. Itoh, T. Fujimoto, M. Furuse, H. Takano, T. Noda, and S. Tsukita. 1998. Occludin-deficient embryonic stem cells can differentiate into polarized epithelial cells bearing tight junctions. *J. Cell Biol*. 141:397–408.

Schneeberger, E. 1994. Tight junctions: their modulation under physiological and pathological states. *In* Molecular Mechanisms of Epithelial Cell Junctions: From Development to Disease. S. Citi, editor. RG Landes Biomedical Publishers, Austin, TX. 123–140.

Shohet, R.V., M.A. Conti, S. Kawamoto, Y.A. Preston, D.A. Brill, and R.S. Adelstein. 1989. Cloning of the cDNA encoding the myosin heavy chain of a vertebrate cellular myosin. *Proc. Natl. Acad. Sci. USA*. 86:7726–7730.

Steinmetz, M.O., A. Stock, T. Schulthess, R. Landwehr, A. Lustig, J. Faix, G. Gerisch, U. Aebi, and R.A. Kammerer. 1998. A distinct 14 residue site triggers coiled-coil formation in cortexillin I. *EMBO (Eur. Mol. Biol. Organ.) J.* 17:1883–1891.

Stevenson, B.R., and B.H. Keon. 1998. The tight junction: morphology to molecules. *Annu. Rev. Cell Dev. Biol*. 14:89–109.

Stevenson, B.R., J.D. Siliciano, M.S. Mooseker, and D.A. Goodenough. 1986. Identification of ZO-1: a high molecular weight polypeptide associated with the tight junction (zonula occludens) in a variety of epithelia. *J. Cell Biol.* 103:755–766.

Takahashi, K., T. Matsuo, T. Katsube, R. Ueda, and D. Yamamoto. 1998. Direct binding between two PDZ domain proteins Canoe and ZO-1 and their roles in regulation of the jun N-terminal kinase pathway in *Drosophila* morphogenesis. *Mech. Dev*. 78:97–111.

Toyofuku, T., M. Yabuki, K. Otsu, T. Kuzuya, M. Hori, and M. Tada. 1998. Direct association of the gap junction protein connexin-43 with ZO-1 in cardiac myocytes. *J. Biol. Chem*. 273:12725–12731.

Tsukamoto, T., and S.K. Nigam. 1997. Tight junction proteins form large complexes and associate with the cytoskeleton in an ATP depletion model for reversible junction assembly. *J. Biol. Chem*. 272:16133–16139.

Turner, J.R., B.K. Rill, S.L. Carlson, D. Carnes, R. Kerner, R.J. Mrsny, and J.L. Madara. 1997. Physiological regulation of epithelial tight junctions is associated with myosin light-chain phosphorylation. *Am. J. Physiol.* 273:C1378–

C1385.

Willott, E., M.S. Balda, A.S. Fanning, B. Jameson, C. Van Itallie, and J.M. Anderson. 1993. The tight junction protein ZO-1 is homologous to the *Drosophila* discs-large tumor suppressor protein of septate junctions. *Proc. Natl. Acad. Sci. USA*. 90:7834–7838.

Woolfson, D.N., and T. Alber. 1995. Predicting oligomerization states of coiled coils. *Protein Sci*. 4:1596–1607.

Yamamoto, T., N. Harada, K. Kano, S. Taya, E. Canaani, Y. Matsuura, A. Mizoguchi, C. Ide, and K. Kaibuchi. 1997. The Ras target AF-6 interacts with ZO-1 and serves as a peripheral component of tight junctions in epithelial cells. *J. Cell Biol*. 139:785–795.

Yamamoto, T., N. Harada, Y. Kawano, S. Taya, and K. Kaibuchi. 1999. In vivo interaction of AF-6 with activated Ras and ZO-1. *Biochem. Biophys. Res. Commun*. 259:103–107.

Yeaman, C., K.K. Grindstaff, and W.J. Nelson. 1999. New perspectives on mechanisms involved in generating epithelial cell polarity. *Physiol. Rev*. 79: 73–98.

Zhadanov, A.B., D.W. Provance, C.A. Speer, J.D. Coffin, D. Goss, J.A. Blixt, C.M. Reichert, and J.A. Mercer. 1999. Absence of the tight junctional protein AF-6 disrupts epithelial cell-cell junctions and cell polarity during mouse development. *Curr. Biol*. 9:880–888.